Membrane Insertion and Dissociation Processes of a Model Transmembrane Helix†

Yoshiaki Yano and Katsumi Matsuzaki*

Graduate School of Biostudies, Kyoto University, Sakyo-ku, Kyoto 606-8501, Japan

Received May 24, 2002; Revised Manuscript Received August 11, 2002

ABSTRACT: An important subject for elucidating membrane protein (MP) folding is how transmembrane helices (TMHs) insert into and dissociate from membranes. We investigated helix dissociation kinetics and insertion topology by means of intervesicular transfer of the fluorophore-labeled completely hydrophobic model transmembrane helix NBD-$(LALAAAA)_3$-NH_2 (NBD = 7-nitro-2-1,3-benzoxadiazol-4-yl). The peptide forms a topologically stable transmembrane helix, which is in a monomer-antiparallel dimer equilibrium [Yano, Y., Takemoto, T., Kobayashi, S., Yasui, H., Sakurai, H., Ohashi, W., Niwa, M., Futaki, S., Sugiura, Y., and Matsuzaki, K. (2002) *Biochemistry 41,* 3073−3080]. The helix transfer kinetics, representing the helix dissociation process, was monitored by fluorescence recovery of the quenched peptide in donor vesicles containing a quencher upon its transfer to acceptor vesicles without the quencher. The transfer kinetics and vesicle concentration dependence demonstrated that the transfer was mediated by monomer in the aqueous phase. Furthermore, the activation enthalpy was estimated to be $+17.7 \pm 1.3$ kcal mol^{-1}. Helix insertion topology, detected by chemical quenching of the NBD group in the outer leaflet by dithionite ions, was found to be controlled by transmembrane electric potential−helix macro dipole interaction. On the basis of these observations, a model for the helix insertion/dissociation processes was discussed.

In the post-genomic era, elucidation of the physical principles of the folding and the stability of proteins is becoming crucial for the prediction of protein structures and functions from the obtained sequence data. In particular, experimentally intractable membrane proteins (MPs[1]), which are considered to comprise about a third of total proteins, are important as the targets of such prediction analyses because more than 50% of human drug targets are G-protein-coupled receptors and ion channels (*1*), representative MPs. The most fundamental framework of MP−membrane interactions involves the thermodynamics of the folding and the bilayer insertion of a peptide that can form an α-helix as well as helix−helix interactions in the membrane phase. However, experimental approaches to these problems have evolved slowly (*2*). Experimental demonstration of the driving forces of helix−helix interactions in membrane environments has recently begun to emerge (*3*−*7*). Although the folding and the membrane binding of amphipathic helix-forming peptides have been thermodynamically characterized (*8*−*10*), those of hydrophobic transmembrane helix (TMH)-forming peptides are generally very difficult to study because of insolubility and aggregation of hydrophobic peptides in the aqueous phase. Several attempts have been made to overcome these difficulties (*11*−*13*).

In this paper, we investigated the dissociation kinetics and the insertion topology of the model TMH, X-$(LALAAAA)_3$-NH_2 [X = Ac (**I**), 7-nitro-2-1,3-benzoxadiazol-4-yl (NBD) (**II**)] (*14*). The 21-residue peptide is exclusively composed of helix-promoting leucine and alanine, and the terminal charges were blocked by acetylation and amidation. No specific interactions in the side chains, such as ion pair, hydrogen bond, or leucine zipper based on heptad repeats (*15*), are expected. This simplest of helices can form a topologically stable TMH and is in a monomer−antiparallel dimer equilibrium, with an association free energy of ~ -3 kcal mol^{-1} in 1-palmitoyl-2-oleoyl-*sn*-glycero-3-phosphocholine (POPC) bilayers at 25 °C. We estimated the helix transfer kinetics between POPC large unilamellar vesicles (LUVs) by fluorescence recovery of **II** upon transfer from donor vesicles containing the NBD quencher, lissamine rhodamine B 1,2-dihexadecanol-*sn*-glycero-3-phosphoethanolamine (Rh-PE), to acceptor vesicles without quencher. The basic approach of the helix transfer was described by Wimley and White in the study of reversible insertion of a model TMH (*11*). The transfer kinetics followed first-order kinetics reflecting the dissociation process. The activation energy of this process was also evaluated. The helix topological preference in the transfer process was examined by quenching of the NBD group in the outer leaflets of LUVs

† Supported in part by the Mitsubishi Foundation, the Kato Memorial Bioscience Foundation, the Japan Securities Scholarship Foundation, and Grant-in-Aids for Scientific Reserch (13024244, 14017048, and 14572091) from the Ministry of Education, Culture, Sports, Science and Technology of Japan.

* To whom correspondence should be addressed. Telephone: 81-75-753-4574. Fax: 81-75-761-2698. E-mail: katsumim@pharm.kyoto-u.ac.jp.

[1] Abbreviations: $DiSC_2(5)$, 3,3′-diethylthiadicarbocyanine iodide; ESR, electron spin resonance; Fmoc, 9-fluorenylmethoxycarbonyl; FRET, fluorescence resonance energy transfer; LUVs, large unilamellar vesicles; MLVs, multilamellar vesicles; MP, membrane protein; NBD, 7-nitro-2-1,3-benzoxadiazol-4-yl; NBD-PE, 1,2-dipalmitoyl-*sn*-glycero-3-phosphoethanolamine-*N*-(7-nitro-2-1,3-benzoxadiazol-4-yl); POPC, 1-palmitoyl-2-oleoyl-*sn*-glycero-3-phosphocholine; Rh-PE, lissamine rhodamine B 1,2-dihexadecanol-*sn*-glycero-3-phosphoethanolamine, triethylammonium salt; RP-HPLC, reverse phase-high performance liquid chromatography; TFE, 2,2,2-trifluoroethanol; TMH, transmembrane helix.

10.1021/bi026191v CCC: $22.00
Published on Web 10/08/2002

by dithionite ions. We found that transmembrane potential could control the helix insertion topology by interaction with the helix macro dipole.

MATERIALS AND METHODS

Materials. A peptide chain was constructed by 9-fluorenylmethyloxycaronyl (Fmoc)-solid-phase synthesis on a Rink amide resin. NBD and acetyl moieties were introduced at the N-terminus with NBD-Cl and acetic anhydride in the presence of diisopropylethylamine, respectively. The peptide resin was treated with trifluoroacetic acid-ethanedithiol (95:5) followed by purification by reversed-phase high performance liquid chromatography (RP-HPLC). The purities of the peptides (>90%) were confirmed by RP-HPLC, amino acid analysis, and ion-spray mass spectroscopy. POPC and valinomycin were obtained from Sigma (St. Louis, MO). Spectrograde chloroform and methanol were products of Nacalai Tesque (Kyoto, Japan). NMR-grade 2,2,2-trifluoroethanol (TFE) was purchased from Aldrich (Milwaukee, WI). 1,2-Dipalmitoyl-*sn*-glycero-3-phosphoethanolamine-*N*-(7-nitro-2-1,3-benzoxadiazol-4-yl) (NBD-PE) was supplied by Avanti Polar Lipids (Alabaster, AL). 3,3′-Diethylthiadicarbocyanine iodide ($DiSC_2(5)$) and lissamine rhodamine B 1,2-dihexadecanol-*sn*-glycero-3-phosphoethanolamine, the triethylammonium salt (Rh-PE), were obtained from Molecular Probes (Eugene, OR). The lipids and the peptides were dissolved in a chloroform/methanol mixture and TFE, respectively. The lipid concentration was determined in triplicate by phosphorus analysis (*16*). The concentration of the fluorophore-labeled peptide (**II**) was determined on the basis of the extinction coefficient in methanol ($\epsilon_{449} = 20\,000\ M^{-1}$), which was obtained by absorbance combined with quantitative amino acid analysis in duplicate.

Vesicle Preparation. Large unilamellar vesicles (LUVs) were prepared by an extrusion method as described elsewhere (*17*). In brief, a lipid/peptide mixed film, after drying under vacuum overnight, was hydrated with Tris-HCl buffer (10 mM Tris/150 mM NaCl/1 mM EDTA, pH 7.4) and vortex-mixed to produce multilamellar vesicles (MLVs). The suspension was subjected to 10 freeze−thaw cycles and then extruded through polycarbonate filters (0.1 μm pore size filters, 31 times).

Intervesicular Transfer of Peptide. Donor POPC LUVs incorporating 0.5 mol % **II** with 1 mol % Rh-PE as NBD quencher were mixed with an excess of POPC acceptor LUVs. The efficiency of peptide transfer from the donor to the acceptor vesicle populations was evaluated by NBD fluorescence recovery as a function of incubation time. NBD fluorescence ($F_i(t)$) was monitored at 555 nm (excited at 450 nm) after spectral subtraction of pure Rh-PE fluorescence on a Shimadzu RF-5300 spectrofluorometer. A slight emission shift (~5 mn) was observed, depending on **II** concentration in the vesicles because of dimerization. The fluorescence intensity at this emission wavelength was the most insensitive (within 5% error) to peptide concentration. Percent transfer was defined with peptide uniform distribution among donor and acceptor vesicles being 100% transfer

$$\%\text{Transfer}\ (t) = \frac{F_i(t) - F_D}{F_A - F_D} \cdot \frac{L_D + L_A}{L_A} \cdot 100 \qquad (1)$$

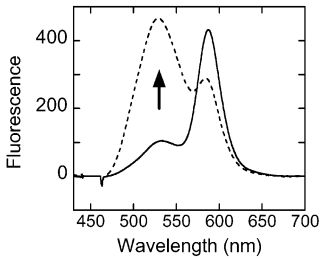

FIGURE 1: FRET from NBD to Rhodamine for measuring the kinetics of **II** transfer between POPC LUVs. Donor POPC vesicles (200 μM) containing 0.5 mol % **II** and 1 mol % Rh-PE were mixed with an excess of acceptor POPC vesicles (1 mM) in 10 mM Tris/150 mM NaCl buffer (pH 7.4) at 25 °C. Emission spectra before (solid trace) and after (broken trace) 24 h incubation are shown. The arrow indicates recovery of NBD fluorescence due to transfer of **II** to acceptor vesicles.

F_D and F_A are experimentally determined fluorescence intensities when all the peptides are in the donor and acceptor vesicles, respectively. L_D and L_A are the lipid concentrations of the donor and acceptor vesicles, respectively.

Detection of Peptide Topology. External addition of dithionite to LUVs chemically quenches the NBD groups in the outer leaflets of the bilayers. After 20 μL of 1 M sodium dithionite/1 M Tris was added to 2 mL of the sample, the time course of NBD fluorescence was monitored at excitation and emission wavelengths of 450 and 533 nm, respectively. The inner leaflet NBD fraction was determined by linearly extrapolating the trace between 150 and 180 s after dithionite addition to 0 s (see Figure 4A).

Transmembrane Potential. Transmembrane potentials of about ±110 mV relative to the external aqueous phase across the bilayer were generated by valinomycin and K^+ concentration gradients. K^+ buffer (10 mM Tris/50 mM K_2SO_4/1 mM EDTA, pH 7.4) and Na^+ buffer (10 mM Tris/50 mM Na_2SO_4/1 mM EDTA, pH 7.4) were used to produce K^+ gradient. In generating an inside-negative potential, a lipid/peptide mixed film was hydrated with the K^+ buffer for the preparation of LUVs. The LUVs were diluted with the Na^+ buffer to produce a K^+ concentration gradient of $[K^+]_{in}/[K^+]_{out} = 100$. The addition of valinomycin dissolved in ethanol at a lipid-to-valinomycin molar ratio of 5000 (~20 valinomycin molecules per LUV on average) was sufficient for potential generation. An inside-positive potential was generated in a similar way by interchanging the K^+ and Na^+ buffers. The potential was calculated from the Nernst equation. The stability of the potential in the presence of the peptide was confirmed by 1 μM voltage-sensitive fluorescent dye, $DiSC_2(5)$ (*18*). The fluorescence was excited at 620 nm and monitored at 670 nm.

RESULTS

Intervesicular Transfer. To detect intervesicular transfer of **II** from the donor to the acceptor vesicles, 1 mol % Rh-PE was incorporated in the donor vesicles as a quencher of the NBD group. Similar techniques have been used to detect intervesicular transfer of fluorescently labeled phospholipids and glycolipids (*19, 20*). The peptide transfer was monitored by NBD fluorescence recovery (Figure 1). The NBD fluorescence (~530 nm) in the donor vesicles was highly quenched (solid trace), whereas a recovery of NBD fluorescence concomitant with a reduction of Rh-PE fluorescence

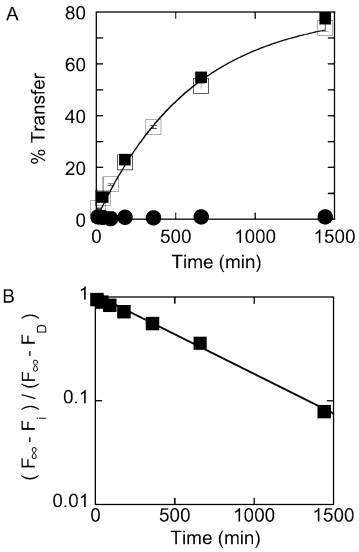

FIGURE 2: Transfer kinetics of **II** at 25 °C. (A) Vesicle concentration dependence of transfer rate. Donor POPC vesicles containing 0.5 mol % **II** and 1 mol % Rh-PE were incubated with acceptor POPC vesicles in a donor-to-acceptor lipid ratio of 1/5 at total lipid concentrations of 1.2 (closed squares) and 12 mM (open squares). The latter sample was diluted 10 times immediately before fluorescence measurement. Percent transfer values were calculated as described under Materials and Methods and are plotted as a function of incubation time. Error bars indicate standard deviations ($n = 2$). NBD-PE transfer in the presence of **I** in the donor vesicles was also examined. Donor vesicles (200 μM) containing 0.5 mol % NBD-PE, 0.5 mol % **I** and 1 mol % Rh-PE were incubated with acceptor POPC vesicles (1 mM) (closed circles). (B) First-order plot of transfer rate. F_∞ shows the fluorescence intensity expected at the equilibrium estimated from Figure 2A.

at 587 nm after 24 h incubation suggested relief from FRET due to the transfer of **II** to the acceptor vesicles (broken trace).

Figure 2A shows the transfer kinetics of **II** at different total vesicle concentrations with the donor-to-acceptor ratio kept at 1:5. The transfer rate of **II** was independent of the vesicle concentration (open vs closed squares). The presence of the peptide might mediate intervesicular exchange of lipids including Rh-PE. To examine this possibility, the transfer of NBD-PE in the presence of 0.5 mol % unlabeled peptide **I** in the donor vesicles was measured. No recovery of NBD-PE fluorescence was observed for 1 day (closed circles in Figure 2). The helix transfer rate of **II** was not affected by the existence of 0.5 mol % **I** in the acceptor vesicles (data not shown). Therefore, the peptide did not perturb the membrane property so as to influence the helix transfer process. The transfer rate obeyed first-order process (Figure 2B) with a transfer rate constant k of 0.10 ± 0.0004 h^{-1} at 25 °C ($n = 2$), corresponding to $t_{1/2} = 600$ min.

Temperature Dependence. Similar experiments were also carried out at 35, 45, and 55 °C. The k values are plotted in the form of the Arrhenius plot (Figure 3). The dissociation rate constant (k) at constant pressure is expressed as (*21*)

$$\ln k = \frac{-\Delta H^{\ddagger\circ}}{RT} + \frac{\Delta S^{\ddagger\circ}}{R} + \ln A \qquad (2)$$

where $\Delta H^{\ddagger\circ}$ and $\Delta S^{\ddagger\circ}$ are the activation enthalpy and entropy, respectively. $\Delta H^{\ddagger\circ}$ ($+17.7 \pm 1.3$ kcal mol^{-1}) can be unambiguously determined from the slope of the Arrhenius plot. However, the constant (so-called preexponential term) A and consequently $\Delta S^{\ddagger\circ}$ are strongly model dependent and cannot be unambiguously established without any reaction model.

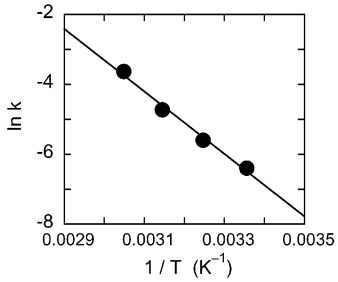

FIGURE 3: Arrhenius plot of the transfer rate constant k (min^{-1}) for **II**. Measurements were performed at 25, 35, 45, and 55 °C ($n = 2$). Error bars (standard deviations) are within the symbols. The linear regression gave a slope of -8940 ± 660 and a y-intercept of 23.5 ± 2.1 ($R = 0.995$).

Helix Insertion and Dissociation Topologies. In POPC bilayers, all peptide molecules were confirmed to form TMHs with either an N-terminus-inside or -outside topology (*14*). The topology of the helix was examined on the basis of the quenching of the NBD group with membrane-impermeable dithionite ions (*22*). Figure 4A shows an example of the time course of NBD fluorescence decrease after dithionite addition. The initial abrupt decrease corresponded to the quenching of the NBD groups in the outer leaflets. The subsequent gradual decrease was assigned to slow permeation of the reducing ion through the peptide-containing membrane (*22*) because the flip-flop motion of the helix was found to be much slower (*14*). The fraction of the inner leaflet NBD group was estimated by the extrapolation indicated by the broken lines and is plotted as a function of incubation time in Figure 4B. The values close to 0.5 during transfer indicate no topological preference in the helix insertion process. Note that these data mainly reflect the helix topology in the acceptor vesicles because an NBD group in the acceptor vesicles shows about 5 times stronger fluorescence than that in the donor vesicles containing the quencher Rh-PE. To obtain information on helix dissociation topology, Rh-PE was incorporated into the acceptor vesicles (Figure 4C). In this case, NBD fluorescence mainly originated from **II** in the donor vesicles. Rh-PE incorporation in the acceptor vesicles had essentially no effect on the helix transfer rate (data not shown). No marked preference of helix topology during transfer was also observed in the helix dissociation process.

Voltage Dependence of Helix Insertion Topology. Membrane electric potentials influence numerous important physiological processes. To examine the membrane potential dependence of helix insertion topology, K^+ diffusion potentials ($\sim\pm 110$ mV) were applied to the acceptor vesicles by K^+ concentration gradients and valinomycin. It was confirmed that the potential was stable at least 3 h in the presence of **II**. Figure 5 shows the effects of transmembrane potential on helix insertion topology during the transfer process. To confirm that the asymmetric ion conditions had no effect on insertion topology, control experiments were performed in the absence of valinomycin (circles in Figure 5). Upon treatment of valinomycin, the N-terminus of the helix preferred the negative potential side both in the cases of inside- and outside-negative potentials, while the helix

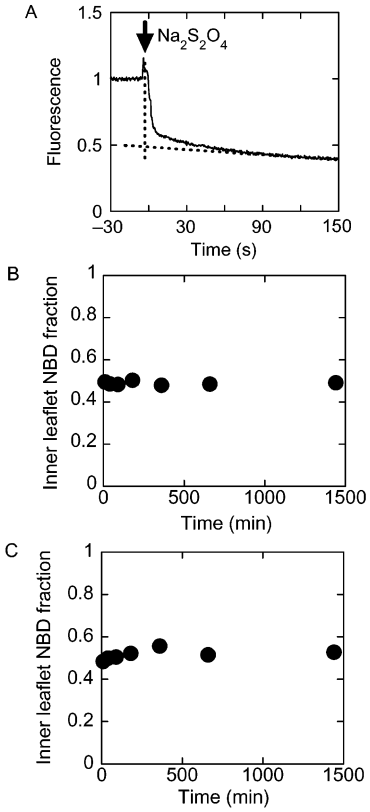

FIGURE 4: Detection of helix topology during the transfer process by the NBD-dithionite reaction. (A) An example of NBD quenching time course. NBD fluorescence at 533 nm (excited at 450 nm) was monitored after sodium dithionite was added at the time indicated by the arrow. The initial abrupt decrease in fluorescence indicates the quenching of the NBD groups exposed to the external aqueous phase. The subsequent gradual decrease was due to the slow membrane permeation of dithionite ions. The helix topology was quantified by extrapolating the linear part of the trace (150−180 s) to the time zero, as shown by the broken lines. (B) Helix insertion topology. Donor POPC vesicles (200 μM) containing 0.5 mol % **II** and 1 mol % Rh-PE were incubated with acceptor POPC vesicles (1 mM) at 25 °C. The fraction of the NBD group in the inner leaflets determined as panel A is plotted as a function of incubation time ($n = 2$). The symbols include error bars (standard deviation). (C) Helix dissociation topology. Donor vesicles (200 μM) with 0.5 mol % **II** were incubated with acceptor vesicles (200 μM) containing 1 mol % Rh-PE. The lower acceptor concentration was chosen to avoid excess reabsorption of NBD fluorescence by Rhodamine (inner filter effect).

transferred from the donor to the acceptor vesicles, indicating that the transmembrane electric field affected the helix insertion topology. The transfer rates were essentially the same as those without membrane potential (data not shown). The fraction of the N-terminal-inside helix in the acceptor vesicles was calculated from the % transfer value and the contribution of **II** in the acceptor vesicles to total fluorescence, indicated in Figure 5. The N-terminus of the helix preferred the negative side of transmembrane potential in negative-to-positive side ratios around 85:15.

DISCUSSION

We investigated intervesicular transfer of a TMH using the FRET technique often utilized to monitor lipid transfer (*19*, *23*). The control experiment using NBD-PE instead of **II** (closed circles in Figure 2A) confirmed that relief from FRET observed for **II** (squares in Figure 2A) truly reflected

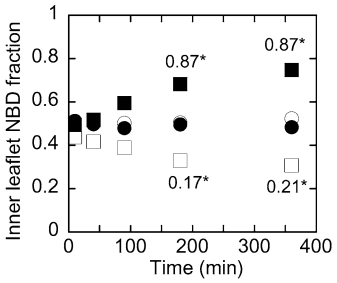

FIGURE 5: Voltage dependence of helix insertion topology. Donor POPC vesicles (200 μM) containing 0.5 mol % **II** and 1mol % of Rh-PE were incubated at 25 °C with acceptor POPC vesicles (1 mM), in which the membrane potential was generated by a K^+ concentration gradient and valinomycin. The fraction of inner leaflet NBD was determined as in Figure 4 at various incubation periods. Open and closed symbols show K^+ -outside and K^+ -inside ion gradients, respectively. Circles denote control experiments in the absence of valinomycin. Under inside potentials of −110 mV (closed squares) and +107 mV (open squares) relative to the outside, calculated from the Nernst equation, the helix topology changed during helix transfer. The numbers marked with asterisks show fractions of NBD inside in the acceptor vesicles calculated from the % transfer value and the contribution of **II** in acceptor vesicles to total fluorescence.

the intervesicular transfer of the peptide and that the peptide induced neither vesicle fusion nor lipid exchange between vesicles.

Mechanism of Peptide Transfer. The peptide transfer between vesicles can occur either via the diffusion of free peptides in solution or upon vesicle collision (*19*). In the latter case, the transfer rate depends on the vesicle concentration. The absence of vesicle concentration dependence of the transfer rate (Figure 2A) clearly indicates that the transfer is mainly mediated by diffusion of free peptide at least in the lipid concentration range investigated (1.2−12 mM). The transfer rate was well fitted by a first-order process (Figure 2B). The rate constant represents that of the dissociation process (*19*). In the membrane environment, the peptide used in this study is mainly in a monomer−antiparallel dimer equilibrium (*14*). The first-order kinetics also suggests that the helix should dissociate into the aqueous phase as a monomer. If the helix had dissociated as a dimer or higher oligomers, the transfer rate would have decreased more rapidly than expected from the first-order kinetics. The conformation of the peptide in the aqueous phase could not be examined because of its very low concentration.

Activated State. The Arrehenius-type plot provides information on thermodynamic parameters related to transition to the activated state. The estimation of the $\Delta S^{\ddagger\circ}$ value requires a specific reaction model. We used Kramers' theory of reaction rate (*24*), which is applicable to reactions in the condensed phase. Activation energies were calculated using a theoretical description used for dissociation of a monomer from a detergent micelle (*25*) or a phospholipid vesicle (*23*). In this model, the monomer is treated as a straight rod moving along its axis perpendicular to the membrane plane (or micelle surface) with a linear reaction coordinate toward its activated state. Despite this simplification, the obtained expression provides a meaningful estimation of activation energies considering friction in a viscous environment. According to this model, A is described as D_m/l_b^2. D_m is the diffusion coefficient for the dissociating monomer, and l_b (Å) is the width of the barrier that is RT energy units below

its maximum. R and T are the gas constant and absolute temperature, respectively. D_m was approximated to the lateral diffusion coefficient of the membrane protein, rhodopsin in dipalmitoylphosphatidylcholine membranes, 1.8×10^{-8} cm^2 s^{-1} (*26*). l_b was assumed to be 1 Å, deduced from the theoretical study on an uncapped 25-polyalanine helix in its activated state (*27*), although recent studies show that polyalanine cannot form a stable transmembrane helix (*28*, *29*). The value of ln A in eq 2 (+23.1) was not very sensitive to the choice of the D_m and l_b values. For example, an l_b value of 2 Å gave the value of +21.7. The obtained thermodynamic parameters for membrane dissociation of the peptide based on this kinetic model were $\Delta H^{\ddagger\circ} = +17.7$ kcal mol^{-1}, $T\Delta S^{\ddagger\circ} = +0.2$ kcal mol^{-1}, and $\Delta G^{\ddagger\circ} = +17.5$ kcal mol^{-1} at 25 °C. This analysis according to Aniansson et al. (*25*) and Nichols (*23*) revealed that the activation free energy of the helix dissociation is predominantly due to the enthalpy of activation. This trend was also observed in the phospholipid dissociation process from the vesicle (*23*). The activation free energy of +17.5 kcal mol^{-1} was comparable to the theoretical energy barrier ~24 kcal mol^{-1} of dissociation of an uncapped membrane-spanning $(Ala)_{25}$ helix along the bilayer normal (*27*), even though in this calculation the membrane was simplified as a slab of low dielectric constant. Recently, the activation energy for insertion of a model TMH was reported to be +22 kcal mol^{-1} (*13*), which is comparable to our estimate for helix dissociation.

Membrane Partitioning of Helix. The determination of the water−membrane partition coefficient of **II** could estimate the insertion rate constant in combination with the dissociation rate constant k, allowing full description of kinetic parameters associated with the membrane insertion/dissociation process of TMH. Furthermore, to predict TMHs in a protein from the amino acid sequence, experimental elucidation of equilibrium thermodynamics of a helix in water−membrane system is essentially important. In particular, the helix backbone contribution remains to be elucidated (*11*, *28*). We tried to determine the helix partition coefficient from the decrease in NBD fluorescence originated from redistribution of the helix between the water and membrane phases upon 500 times dilution of **II** incorporated in 50 mM LUVs (data not shown). However, no detectable decrease (>1%) in the fluorescence was observed after 60 min incubation after correcting for a slight fluorescence decrease due to adsorption of the peptide to the quartz cell walls, indicating that the helix partition free energy is more negative than −10.5 kcal mol^{-1}.[2] Together with the activation free energy estimate, the actual partition free energy of the helix appears to be in the range of −10.5 to −17.5 kcal mol^{-1}. This estimate was larger in magnitude among experimental and theoretical values reported for various TMHs, such as the model TMH TMX-1 (−7.1 kcal mol^{-1}) (*11*) and one of the TMHs of the M13 coat protein (−12 kcal mol^{-1}) (*30*), $(Ala)_{25}$ (−4 kcal mol^{-1}) (*27*). The helix backbone (glycyl unit) transfer free energy of **II** estimated using the side chain hydrophobicity scale based on water−octanol partitioning (*31*) was 0.6−0.3 kcal mol^{-1} per residue.[3] This value is significantly lower than the best current estimates (~2 kcal mol^{-1}) (*27*, *28*, *32*). It should be noted that the above estimates of various ΔG values suffer from uncertainties, e.g., regarding conformation and aggregation in the aqueous phase (*2*, *32*).

Helix Topology. A helix has a macro dipole moment with ± 0.5 e at its termini (*33*). The dipole moment likely interacts with electric potentials within the lipid bilayers (*34*). The hydrocarbon core of a phosphatidylcholine bilayer is suggested to have a large positive potential of several hundred mV (dipole potential) originating from the C═O groups and/or water hydrated to the headgroup (*35*). The dipole potential facilitates the transport of anions across bilayers compared with cations (*36*, *37*). Therefore, this potential should raise the energy of the N-terminal end of a helix crossing the bilayer by ca. 5 kcal mol^{-1} (200 mV × Faraday constant) relative to the C-terminal end (*38*). However, no specific topological preference was observed in the helix dissociation or insertion process (Figure 3). The helix may locally perturb the bilayer structure, diminishing the dipole potential. The larger hydrophobicity of the N-terminus containing NBD and Leu may also contribute to the compensation of the putative dipole potential effect. The transfer free energy of NBD-Cl and Leu from water to 1-octanol is ~5 kcal mol^{-1} larger than that of Ala (*31*, *39*).

The transmembrane potential is also considered to interact with the helix dipole (*34*). In particular, this topic has been extensively discussed in relation to the voltage-gating mechanisms of channel-forming peptides (*33*, *38*). In this study, we directly demonstrated that the simplest of helices interacts with transmembrane potential (Figure 5). A transmembrane potential of 110 mV prefers helices with their dipole moments antiparallel to the potential over parallel helices in a ratio of about 85:15, which corresponds to a free energy difference between the two orientations of ~1 kcal mol^{-1} (RT ln(85/15)), if equilibrium is assumed. A theoretical study evaluated an energy difference of about 2 kcal mol^{-1} at 100 mV for an $(Ala)_{12}$ helix (*40*). Our smaller value may be due to a reduction in the effective charges at the termini by partial hydration or our measurement reflected a kinetically trapped topology in the insertion process, because the flip-flop of the helix did not occur (*14*) (also, vide infra).

Model for Helix Insertion and Dissociation. Our data are consistent with the idea of a metastable interface state in which coupled interfacial partitioning/folding occurs (*2*, *32*, *41*), as indicated in Figure 6A. This model can be compared with a theoretical study of the uncapped $(Ala)_{25}$ helix insertion into bilayers (*27*). In this study, even if the peptide

[2] The peptide partition free energy ΔG was calculated from the mole-fraction partition coefficient K as $\Delta G = -RT$ ln K, assuming the redistribution of 1% of the peptide molecules in the membrane (50 mM LUVs) to the aqueous phase upon 500 times dilution. Before dilution, K is described as $\{(1 - X)/(50 \times 10^{-3})\}/(X/55.5)$, where X is the fraction of the peptide in the aqueous phase. The mole concentration of water is 55.5 M. K after dilution is given by $\{0.99(1 - X)/(50 \times 10^{-3}/500)\}/[\{0.01(1 - X) + X\}/55.5]$. Under these conditions, the X and K values are evaluated as 0.2×10^{-4} and 55×10^6, respectively.

[3] The contribution of the NBD group was not included because this moiety is mostly exposed to water (*14*).

[4] Free energy contributions from lipid perturbation (~2 kcal mol^{-1}) and immobilization (~5 kcal mol^{-1}) were not included in these values (42).

[5] The helix transfer through the aqueous phase is apparently incompatible with no flip-flop of the helix observed in the previous study (*14*). However, we found that dithionite pretreatment of LUVs used in the flip-flop study largely suppressed helix dissociation (data not shown), for unknown reasons. The extent of suppression depended on the conditions of dithionite pretreatment (concentration, reaction time, temperature, and so on). Apparent flip-flop was observed only accompanied with the helix transfer (data not shown).

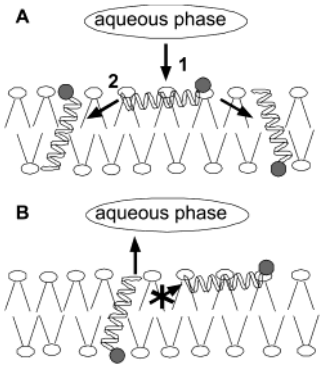

FIGURE 6: Schematic illustration of membrane insertion (A) and dissociation (B) processes for the helix **II**. The gray ball represents the NBD group attached at the N-terminus.

already takes a helix in the aqueous phase, the interfacial state is in a deep free energy minimum (∼14 kcal mol^{-1})[4] because the helix dipole is mostly hydrated whereas the Ala side chains in one face of the helix are buried. If the helix vertically inserts along the bilayer normal, free energy increases with insertion until the energy barrier (∼12 kcal mol^{-1}) without an energy minimum. The interfacial state is metastable, and therefore transient, because such a state could not be detected (*14*). This insertion model is in keeping with the helix dipole−transmembrane potential interactions (Figure 5): The helix is already formed in the interfacial region prior to insertion and has one terminus "swing around" so as to penetrate the bilayer (*27*) by sensing the potential. The energy barrier from the interfacial state to the transmembrane state should be much smaller than the activation energy of dissociation (+17.5 kcal mol^{-1}) because the dissociation process was rate-limiting in the intervesicular transfer process.

In contrast to the insertion process, the helix appears to dissociate from the membrane without passing through the interface state (Figure 6B) because the helix flip-flop motion is much slower than the transfer rate (*14*).[5] One explanation is that conversion from the vertical to the horizontal orientation would require a significant energy cost due to elastic deformation or disordering of bilayers upon tilting or rotating the helix axis (*42*).

REFERENCES

1. Russell, R. B., and Eggleston, D. S. (2000) New roles for structure in biology and drug discovery, *Nat. Struct. Biol. 7 (Suppl.)*, 928−930.
2. White, S. H., and Wimley, W. C. (1998) Hydrophobic interactions of peptides with membrane interfaces, *Biochim. Biophys. Acta 1376*, 339−352.
3. Choma, C., Gratkowski, H., Lear, J. D., and DeGrado, W. F. (2000) Asparagine-mediated self-association of a model transmembrane helix, *Nat. Struct. Biol. 7*, 161−166.
4. Gratkowski, H., Lear, J. D., and DeGrado, W. F. (2001) Polar side chains drive the association of model transmembrane peptides, *Proc. Natl. Acad. Sci. U.S.A. 98*, 880−885.
5. Zhou, F. X., Cocco, M. J., Russ, W. P., Brunger, A. T., and Engelman, D. M. (2000) Interhelical hydrogen bonding drives strong interactions in membrane proteins, *Nat. Struct. Biol. 7*, 154−160.
6. Zhou, F. X., Merianos, H. J., Brunger, A. T., and Engelman, D. M. (2001) Polar residues drive association of polyleucine transmembrane helices, *Proc. Natl. Acad. Sci. U.S.A. 98*, 2250−2255.
7. Mall, S., Broadbridge, R., Sharma, R. P., East, J. M., and Lee, A. G. (2001) Self-association of model transmembrane α-helices is modulated by lipid structure, *Biochemistry 40*, 12379−12386.
8. Wieprecht, T., Beyermann, M., and Seelig, J. (1999) Binding of antibacterial magainin peptides to electrically neutral membranes: thermodynamics and structure, *Biochemistry 38*, 10377−10387.
9. Ladokhin, A. S., and White, S. H. (1999) Folding of amphipathic α-helices on membranes: energetics of helix formation by melittin, *J. Mol. Biol. 285*, 1363−1369.
10. Wieprecht, T., Apostolov, O., Beyermann, M., and Seelig, J. (2000) Membrane binding and pore formation of the antibacterial peptide PGLa: thermodynamic and mechanistic aspects, *Biochemistry 39*, 442−452.
11. Wimley, W. C., and White, S. H. (2000) Designing transmembrane α-helices that insert spontaneously, *Biochemistry 39*, 4432−4442.
12. Hunt, J. F., Rath, P., Rothschild, K. J., and Engelman, D. M. (1997) Spontaneous, pH-dependent membrane insertion of a transbilayer α-helix, *Biochemistry 36*, 15177−15192.
13. Meijberg, W., and Booth, P. J. (2002) The activation energy for insertion of transmembrane α-helices is dependent on membrane composition, *J. Mol. Biol. 319*, 839−853.
14. Yano, Y., Takemoto, T., Kobayashi, S., Yasui, H., Sakurai, H., Ohashi, W., Niwa, M., Futaki, S., Sugiura, Y., and Matsuzaki, K. (2002) Topological stability and self-association of a completely hydrophobic model transmembrane helix in lipid bilayers, *Biochemistry 41*, 3073−3080.
15. Cohen, C., and Parry, D. A. (1990) α-helical coiled coils and bundles: how to design an α-helical protein, *Proteins 7*, 1−15.
16. Bartlett, G. R. (1959) Phosphorus assay in column chromatography, *J. Biol. Chem. 234*, 466−468.
17. Matsuzaki, K., Murase, O., Fujii, N., and Miyajima, K. (1996) An antimicrobial peptide, magainin 2, induced rapid flip-flop of phospholipids coupled with pore formation and peptide translocation, *Biochemistry 35*, 11361−11368.
18. Sims, P. J., Waggoner, A. S., Wang, C. H., and Hoffman, J. F. (1974) Studies on the mechanism by which cyanine dyes measure membrane potential in red blood cells and phosphatidylcholine vesicles, *Biochemistry 13*, 3315−3330.
19. Nichols, J. W., and Pagano, R. E. (1982) Use of resonance energy transfer to study the kinetics of amphiphile transfer between vesicles, *Biochemistry 21*, 1720−1726.
20. Mattjus, P., Kline, A., Pike, H. M., Molotkovsky, J. G., and Brown, R. E. (2002) Probing for preferential interactions among sphingolipids in bilayer vesicles using the glycolipid transfer protein, *Biochemistry 41*, 266−273.
21. Atkins, P. W. (1990) Molecular Reaction Dynamics, in *Physical Chemistry*, 4th ed., pp 840−872, Oxford University Press, Oxford.
22. McIntyre, J. C., and Sleight, R. G. (1991) Fluorescence assay for phospholipid membrane asymmetry, *Biochemistry 30*, 11819−11827.
23. Nichols, J. W. (1985) Thermodynamics and kinetics of phospholipid monomer-vesicle interaction, *Biochemistry 24*, 6390−6398.
24. Kramers, H. A. (1940) Brownian motion in a field of force and the diffusion model of chemical reactions, *Physica 7*, 284−304.
25. Aniansson, E. A. G., Wall, S. N., Almgren, M., Hoffmann, H., Kielmann, I., Ulbricht, W., Zana, R., Lang, J., and Tondre, C. (1976) Theory of the kinetics of micellar equilibria and quantitative interpretation of chemical relaxation studies of micellar solutions of ionic surfactants, *J. Phys. Chem. 80*, 905−922.
26. Vaz, W. L., Criado, M., Madeira, V. M., Schoellmann, G., and Jovin, T. M. (1982) Size dependence of the translational diffusion of large integral membrane proteins in liquid-crystalline phase lipid bilayers. A study using fluorescence recovery after photobleaching, *Biochemistry 21*, 5608−5612.
27. Ben-Tal, N., Ben-Shaul, A., Nicholls, A., and Honig, B. (1996) Free-energy determinants of α-helix insertion into lipid bilayers, *Biophys. J. 70*, 1803−1812.
28. Jayasinghe, S., Hristova, K., and White, S. H. (2001) Energetics, stability, and prediction of transmembrane helices, *J. Mol. Biol. 312*, 927−934.
29. Lewis, R. N., Zhang, Y. P., Hodges, R. S., Subczynski, W. K., Kusumi, A., Flach, C. R., Mendelsohn, R., and McElhaney, R. N. (2001) A polyalanine-based peptide cannot form a stable transmembrane α-helix in fully hydrated phospholipid bilayers, *Biochemistry 40*, 12103−12111.
30. Soekarjo, M., Eisenhawer, M., Kuhn, A., and Vogel, H. (1996) Thermodynamics of the membrane insertion process of the M13 procoat protein, a lipid bilayer traversing protein containing a leader sequence, *Biochemistry 35*, 1232−1241.

31. Wimley, W. C., Creamer, T. P., and White, S. H. (1996) Solvation energies of amino acid side chains and backbone in a family of host−guest pentapeptides, *Biochemistry 35*, 5109−5124.
32. White, S. H., and Wimley, W. C. (1999) Membrane protein folding and stability: physical principles, *Annu. Rev. Biophys. Biomol. Struct. 28*, 319−365.
33. Sansom, M. S. (1991) The biophysics of peptide models of ion channels, *Prog. Biophys. Mol. Biol. 55*, 139−235.
34. Cafiso, D. S. (1991) Lipid bilayers: membrane-protein electrostatic interactions, *Curr. Opin. Struct. Biol. 1*, 185−190.
35. Zheng, C., and Vanderkooi, G. (1992) Molecular origin of the internal dipole potential in lipid bilayers: calculation of the electrostatic potential, *Biophys. J. 63*, 935−941.
36. Honig, B. H., Hubbell, W. L., and Flewelling, R. F. (1986) Electrostatic interactions in membranes and proteins, *Annu. Rev. Biophys. Biophys. Chem. 15*, 163−193.
37. Franklin, J. C., and Cafiso, D. S. (1993) Internal electrostatic potentials in bilayers: measuring and controlling dipole potentials in lipid vesicles, *Biophys. J. 65*, 289−299.
38. Cafiso, D. S. (1994) Alamethicin: a peptide model for voltage gating and protein-membrane interactions, *Annu. Rev. Biophys. Biomol. Struct. 23*, 141−165.
39. Materazzi, S., Curini, R., Gabrielli, M. G., Fava, L., and Menghi, G. (1994) Quantitative and qualitative fluctuation of water in the mouse submandibular gland under secretagogue effect, *Cell. Mol. Biol. (Noisy-le-grand) 40*, 787−794.
40. Roux, B. (1997) Influence of the membrane potential on the free energy of an intrinsic protein, *Biophys. J. 73*, 2980−2989.
41. Jacobs, R. E., and White, S. H. (1989) The nature of the hydrophobic binding of small peptides at the bilayer interface: implications for the insertion of transbilayer helices, *Biochemistry 28*, 3421−3437.
42. Ben-Shaul, A., Ben-Tal, N., and Honig, B. (1996) Statistical thermodynamic analysis of peptide and protein insertion into lipid membranes, *Biophys. J. 71*, 130−137.

BI026191V